JOURNAL OF CATALYSIS 47, 214–231 (1977)

Chemisorption and Reaction of Acetylene and Ethylene on the α-Fe(100) Clean Iron Surface[1]

CHARLES BRUCKER AND THOR RHODIN[2]

School of Applied and Engineering Physics, Cornell University, Ithaca, New York 14853

Received September 22, 1976; revised January 7, 1977

Photoemission electron spectroscopy in the vacuum ultraviolet range (UPS) with LEED-Auger is used to study chemisorption and reaction of acetylene and ethylene on both clean and partially deactivated single crystal α-Fe(100) surfaces. The molecular orbital valence electronic structure is used to elucidate the electronic nature of the bonding mechanism, and to infer changes in the geometrical structure of the molecule upon chemisorption. Carbon–carbon scission is induced for both acetylene and ethylene chemisorption on the highly active clean surface, even at low temperatures. Distinctive spectral features indicate molecular conversion to CH_n (n = 1, 2) and other fragmented species possibly unique to surface-stabilized complexes. Under certain conditions a proposed transitional multicomponent state is observed. It is postulated that a weakly bonded molecular layer forms above the layer of chemisorbed fragments, or on surfaces which have been partially deactivated by prechemisorption of carbon or oxygen atoms. Perturbations of the nonbonding σ-levels imply geometrical distortions involving stretching and bending of the weakly chemisorbed molecules. The degree of distortion serves as a measure of the reactivity of the surface for chemisorptive phenomena involving unsaturated molecules. It is postulated that bonding patterns for olefins on transition metal surfaces are comparatively similar to those found in organometallic and cluster compounds.

I. INTRODUCTION

An understanding of the reactivity of transition metal surfaces during chemical bond formation with unsaturated molecules, such as alkenes and alkynes, is fundamental to clarification of the role transition metals, particularly iron, play in heterogeneous catalytic processes. Many useful comparisons can be made to the available broad information on organometallic chemistry and to more recent results on cluster chemistry. Little is known, however, about the effect of the detailed crystallography and activation state of the surface on chemical bonding and molecular distortion.

Clean and partially deactivated surfaces of iron of known structure and composition can now be prepared which show varying chemical reactivity towards unsaturated hydrocarbon molecules ranging from strong chemisorption to very weak molecular chemisorption. Systematic changes in both the electronic and geometric aspects of the chemisorbed state as the chemical nature of the surface is varied in a controlled fashion can be correlated with details of the surface valence electronic structure.

Each particular compositional-configurational state of the iron surface gives rise to a unique distribution in space and

[1] Supported by the Materials Science Center of Cornell University and the American Iron and Steel Institute.

[2] Address inquiries to this author.

ISSN 0021-9517

energy of surface valence electrons. It is the surface valence electronic structure which largely determines the physical and chemical nature of bonding at surfaces. Ultraviolet photoemission spectroscopy (UPS) is a versatile surface-sensitive probe of the occupied valence electronic orbitals for both the clean and chemisorbed surface. UPS was used in conjunction with LEED-Auger spectroscopy to study electronic and geometric effects during the chemisorption and reaction of acetylene and ethylene on clean as well as partially deactivated α-Fe(100) surfaces. A preliminary presentation of some of this work was made by Anderson *et al.* (*1*), with specific reference to theoretical calculations of hydrocarbon configurations at low temperatures. A more detailed discussion of the energy levels of the various surface–molecule combinations will be published separately (*2*).

II. EXPERIMENTAL TECHNIQUE

1. Experimental System

The experimental system has been described previously (*3*). A conventional four-grid LEED/Auger spectrometer, modified for UPS experiments by the addition of a cold cathode helium discharge light source giving monochromatic radiation at 21.2 eV, was used to perform all energy analyses. With the light source in operation, the pressure rose from a base of 1×10^{-10} to 5×10^{-9} Torr, due primarily to residual helium gas. Photons and helium atoms incident on the sample could be interrupted to allow controlled dosing procedures, or during photodissociation/desorption tests, by a straight-through valve separating the light source from the sample chamber. All the present work was obtained at a light incidence angle of 40° from the surface normal. A total photocurrent of $2–3 \times 10^{-9}$ A resulted in measurement periods for the angle-averaged spectra on the order of 1–10 min. A computerized data acquisition and storage system with graphic display (DEC GT-40) greatly facilitated the accumulation of data and precise subtraction of spectra to obtain difference curves. Data acquisition was optimized to the point where electronic noise was reduced in general to a negligible fraction of the measured intensities.

Acetylene (C_2H_2) and ethylene (C_2H_4) were stored in Pyrex flasks (Airco, nominal purity 99.5%) and introduced to the sample chamber via sapphire-sealed controlled-leak valves (Varian). Dosing was achieved by leaking gas to a given pressure–time product, e.g., a 1 L exposure (1 L = 10^{-6} Torr-sec) was obtained by leaking gas to a pressure of 5×10^{-8} Torr for 20 sec. The sample temperature above room temperature was measured using a Pt–Pt 10% Rh thermocouple spot-welded to the reverse side of the crystal. When cooling the sample with liquid nitrogen, the temperature was monitored with a calibrated platinum resistor, clamped onto the same cooling reservoir that the crystal leads were attached to. In this way, reasonably accurate temperature measurements (± 5 K) could be obtained once equilibrium conditions were established. During all low temperature experiments a liquid nitrogen-cooled trap in the chamber pump manifold was kept filled.

2. Surface Preparation

Crystal growing procedures and methods used to obtain the clean Fe(100) surface are discussed in Ref. (*3*). Iron is difficult to clean not only because it is very reactive chemically but also because the lattice of the allotropic form α (bcc, lattice constant $a = 2.87$ Å) is stable only below 910°C. Thus, the crystal growing and surface cleaning procedures must be done below this temperature. We review the preparation of the clean surface briefly, with emphasis on refinements in the

cleaning technique particularly relevant to this study.

After insertion into the UHV system, bakeout, and degassing at ~600°C for several hours, the initial surface contaminants detected by AES were phosphorus, sulfur, carbon, nitrogen and oxygen. Sputter-annealing removed all impurities except carbon, which in turn could be removed by heat treatment in oxygen. Alternatively, it was found that small residual amounts of chemisorbed oxygen could be effectively removed by gas phase titration using acetylene or ethylene. Presumably, chemisorbed carbon and oxygen atoms are catalytically activated by gentle heating to 500°C to form CO or CO_2, which is subsequently desorbed; the reaction proceeds until one of the reactants in the surface region in exhausted.

Analysis of the amplitudes of the AES impurity peaks for the clean surface indicated surface concentrations of 1–3% of a monolayer each for carbon, nitrogen, and oxygen (curve a, Fig. 1). The corresponding LEED pattern was a sharp $p(1 \times 1)$. Attempts at obtaining lower level Auger spectra were obscured by partly unavoidable AES electron beam effects, e.g., carburization of the surface in the vicinity of the irradiated area (*3*). Thus, the completely clean surface suffered small recontamination as the AES spectrum was being recorded.

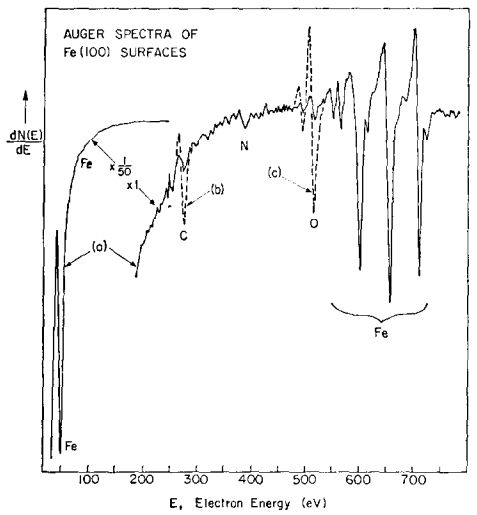

FIG. 1. Derivative Auger spectra for (a) cleaned surface, (b) carbon-deactivated surface, and (c) oxygen-deactivated surface. Not indicated is the complete disappearance of the O-signal in spectrum (b), and similarly the disappearance of the C-signal in spectrum (c). (Primary beam energy 3000 eV; modulation 10 V peak-to-peak.)

This and other limitations inherent to electron beam effects have been avoided in this study by using UPS to monitor surface composition in the final stages of preparation. This requires a knowledge of the valence impurity-induced levels in the UPS spectrum and the ability to deduce quantitative trace impurity concentrations based on these levels. Chemisorbed oxygen on α-Fe(100) is ideally suited for this sort of application. The $O(2p)$ resonance level in the UPS spectrum is clearly defined against a smooth slowly varying background emission. Hence, a calibration scheme for accurately determining the oxygen coverage from the normalized peak area was developed as part of an in-depth study of the interaction of oxygen with Fe(100) (*3*). In direct comparison with AES-compositional analysis, it appears that UPS analysis can be equally if not more sensitive to trace oxygen impurity on Fe(100) (*3*). On the other hand, the small photoionization cross section for chemisorbed carbon makes UPS particularly insensitive to its presence. Thus, to insure against carbon contamination, heat treatment in oxygen was continued until a trace amount of chemisorbed oxygen was present as judged by UPS. This then implied the complete removal of carbon via thermally activated surface titration followed by desorption of CO or CO_2, as previously mentioned. In this manner a surface virtually free of carbon and with an oxygen impurity level comparable to or less than that found in the AES analysis could be obtained. Using UPS as a cleanliness monitor also elimi-

nated uncertainties associated with the precise location of the photon beam on the same area of the crystal as the AES electron beam.

III. PARTIALLY DEACTIVATED SURFACES

In order to study changes in hydrocarbon chemisorptive behavior as a function of surface reactivity, we also prepared surfaces intentionally partially deactivated with approximately one monolayer of chemisorbed carbon or oxygen atoms. The Auger spectra corresponding to these surfaces are shown in Fig. 1, where we note that on the carbonated surface the oxygen signal completely disappeared, and similarily on the oxidized surface the carbon signal completely disappeared. Both carbon and oxygen chemisorbed overlayers exhibit $c(2 \times 2)$ LEED patterns at coverages giving Auger peak heights half as great as those shown in Fig. 1. Since the $c(2 \times 2)$ pattern corresponds to one chemisorbed atom to two substrate atoms (*3*), the spectra in Fig. 1 should correspond roughly to monolayer coverage. In the case of oxygen, UPS measurements provide additional coverage confirmation (*3*). UPS spectra also indicate the formation of FeO iron oxide at monolayer coverage (*3*). A LEED structural analysis of oxygen on Fe(100) shows the preferred sites for the oxygen atoms are the four-coordinate holes (*4*). Whether or not this is true for carbon is not yet known by LEED structural analysis.

Knowledge of the exact coverage is not as critical as is the excellent reproducibility of each surface by simply flashing to 500°C after an adsorption run. The carbonated surface showed very little change in coverage or activity following many hydrocarbon adsorption and flash-off cycles. Similarly, the oxidized surface showed very little alteration in coverage. In fact, heat treatment in acetylene or ethylene is ineffective for removing iron oxide (FeO) itself. It must be sputtered to regain the clean surface. Also, it will be shown that hydrocarbon adsorption on these surfaces can be characterized as very weak molecular chemisorption. We thus denote these surfaces as "partially deactivated," in contrast to the highly reactive clean surface.

IV. EXPERIMENTAL RESULTS

1. Acetylene

UPS spectra for the adsorption of acetylene on the clean Fe(100) surface as a function of coverage, time and temperature are shown in Fig. 2. The spectra are plotted with the electron binding energy referred to the Fermi cut-off, E_F. Part 1 of this figure shows the sequential dosing of acetylene onto the clean surface at 98 K. The clean surface spectrum exhibits iron *d*-band emission within ~4 eV of E_F and a weak level at ~5.3 eV due to a small amount of residual chemisorbed oxygen. The coverage, estimated from the area of this oxygen contaminant level, is less than 0.025 monolayers [see Ref. (*3*)]. For exposures less than 1.5 L, the most significant spectral changes are an attenuation of *d*-band emission near E_F and a nearly uniform increase in background intensity at greater binding energies, with weak adsorbate-induced levels apparent at about 5.5 and 10.5 eV (peaks A and C, respectively). With increasing exposure these levels grow dramatically until saturation coverage is quickly reached at 3.5 L exposure (curve 1c). At saturation, a weak adsorbate-induced level at ~12.5 eV is also observed (peak D). The work function change at saturation is $\Delta\phi = -0.5$ eV, obtained by measuring the change in width of the photoemission spectrum.

In addition to peaks, A, C, and D, a level at ~7.5 eV (peak B) is apparent in curve 1c. This is observed to grow at the expense of the other levels, most notably peaks A and C, with increasing time at constant temperature. An intermediate stage in this gradual conversion

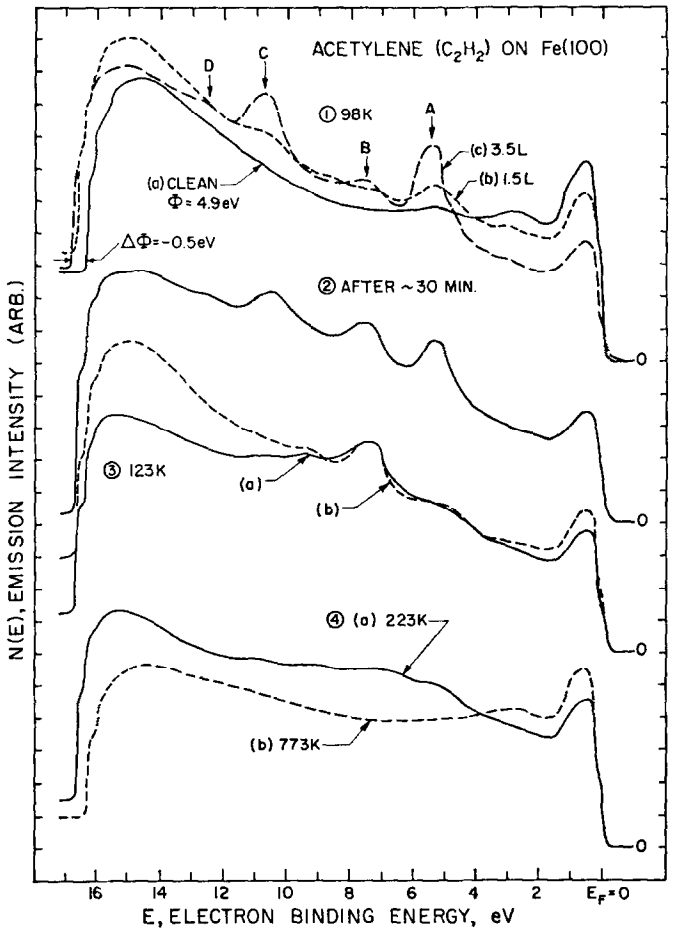

FIG. 2. UPS spectra ($\hbar\omega$ = 21.2 eV) for acetylene adsorbed on a clean Fe(100) surface as a function of time and temperature. (1) Sequential exposure (1 L = 10^{-6} Torr/sec) of acetylene onto the clean surface at 98 K. Work function change, $\Delta\phi$, indicated for saturation exposure (3.5 L); (2) adsorption as in (1c) followed by 30 min wait at 98 K with uv-light source valved off; (3a) after warming the surface in (2) to 123 K or (b) direct adsorption (6 L) onto the clean surface at 123 K; (4) after warming the surface in (3a) to (a) 223 K and (b) 773 K.

process is shown in curve 2, recorded about 30 min after curve 1c was taken. It is important to note that during this period the uv-light source was valved off from the main chamber so that no photons or helium atoms could impinge on the adsorbed overlayer. We also note that as peak B grows in magnitude relative to peaks A and C, no shifts in energy of any of the peak positions are observed, and the conversion is temperature irreversible.

By warming from 98 to 123 K the conversion process is driven rapidly to completion. At this point peak B is seen to be the dominating spectral feature (curve 3a). It is significant that direct adsorption at 123 K (curve 3b) produces essentially the same spectral features as in curve 3a, except for increase in background intensity in the region of strong secondary scattered emission (~10–16 eV) and a slight enhancement of *d*-band emission near E_F. The difference in secondary emission between curves 3a and 3b, Fig. 2, is probably due to an experimental artifact of the retarding grid analyzer. [Note that $N(E)$ at the low energy cut-off also differs for these two curves by about the same

amount. The failure of $N(E)$ to return to zero intensity at the low energy cut-off has been observed in other retarding grid systems as well (*5*), and is thought to be due in part to space charge build-up in the region between the sample and first grid.] It is also noteworthy that the essential features of curve 2 can be reproduced by the appropriate linear combination of curves 1c and 3a.

Further warming to 223 K (curve 4a) produced a broad and rather featureless band of emission from about 4 to 12 eV below E_F. Between 223 and 773 K this band of emission gradually diminished in intensity without the development of any well-defined additional spectral features. Heating to 773 K produced a spectrum (curve 4b) much like that for the clean surface except for subtle differences in the region of iron *d*-band emission. This we attribute to the presence of chemisorbed carbon atoms. It should be noted that the $C(2p)$ level is difficult to detect since it is superimposed on Fe *d*-band emission at about 3 eV. It is not readily apparent unless the surface is more heavily carbonated (e.g., see Fig. 4 and the discussion below).

It is interesting to note that the $O(2p)$ level at ~5.3 eV in curve 4b has disappeared, i.e., the sequence of acetylene adsorption followed by heating, as depicted in Fig. 2, has served to effectively remove the chemisorbed oxygen. Alternatively, excess carbon on the surface can be removed by heat treatment in oxygen, as previously mentioned. The ability to remove oxygen and carbon from the surface at temperatures low enough to inhibit surface segregation of phosphorus and sulfur is essential to the preparation of a completely clean surface.

2. Ethylene

Ethylene adsorption has been followed in a similar manner as shown in Fig. 3, which includes, in addition, results for adsorption onto an oxidized Fe(100) surface. Preparation of the oxidized surface is described subsequently. As before, the clean surface spectrum (curve 1a) exhibits a weak level at ~5.3 eV due to a trace amount of residual oxygen impurity. Saturation exposure of ethylene (curve 1c) produces four adsorbate-induced levels at about 4.5, 6.5, 8.5, and 9.5 eV (peaks A, B, C, and D, respectively). Peaks C and D are more clearly resolved in the difference spectrum shown in Fig. 5. The work function change at saturation is $\Delta\phi = -0.5$ eV. For low exposure (curve 1b) we find that the adsorbate-induced levels are weak, poorly defined, and bear little resemblance to a simple scaled-down version of the spectral features at saturation. Rather, as in the case of acetylene, the chief spectral changes may be described as an attenuation of *d*-band emission near E_F and an overall increase in background intensity at greater binding energies.

We observe little if any change in curve 1c, Fig. 3, with increasing time at a constant temperature of 98 K, up to a period of about 30 min. It is impractical to observe the surface in this stagnant situation for longer time periods since coadsorption of residual background gases tends to become significant. A warming of only 10 degrees, however, is sufficient to initiate a reactivation process analogous to that which occurs for acetylene. Warming to 123 K drives this conversion process rapidly to completion. In this case, curve 2 is obtained, where once again the dominant spectral feature is a broad level at ~7.5 eV (peak E). Essentially, the same curve is obtained by direct adsorption of ethylene at 123 K. Subtle differences between curve 2, Fig. 3, for ethylene and correspondingly curve 3b, Fig. 2, for acetylene, are illustrated in Fig. 4 and discussed below. Further heating to 223 K leads to a broad featureless band of emission similar to that observed in the acetylene adsorption system. Finally, heating to 773 K leaves only carbon on the surface.

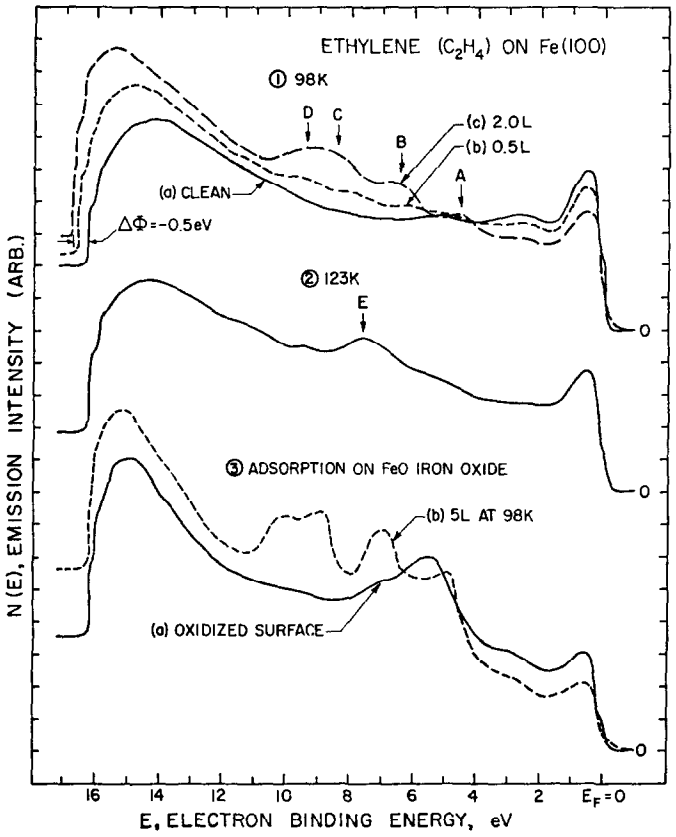

FIG. 3. UPS spectra ($\hbar\omega$ = 21.2 eV) for ethylene adsorbed on clean and oxidized Fe(100) surfaces. (1) Sequential exposure of ethylene onto the clean surface at 98 K. Work function change indicated for saturation exposure (2 L); (2) after warming the surface in (1c) to 123 K; (3) exposure of the oxidized surface (a) to 5 L ethylene at 98 K (b).

It is interesting to see in comparison to the completely clean surface adsorption how the spectral features change when acetylene or ethylene is adsorbed on a partly oxidized Fe(100) surface. The results for ethylene are shown in curves 3a, b, Fig. 3; the results for acetyelene are included below in the difference spectra of Fig. 5. The oxidized iron surface (curve 3a) is prepared under conditions known to produce a two dimensional (FeO) iron oxide film approximately one layer thick [6 L O_2 at room temperature; see previous discussion and Ref. (*3*)]. A large $O(2p)$ resonance level is apparent at ~5.5 eV; the detailed origin of this and other structure is discussed in Ref. (*3*). For saturation coverage of ethylene, the UPS spectrum (curve 3b) exhibits four adsorbate-induced peaks which appear to show a one-to-one correspondence with those observed for adsorption onto the clean surface (curve 1c). There are, however, small but important differences between curves 3b and 1c both in absolute peak positions with reference to the vacuum level and in relative peak spacings. A discussion of the significance of these differences with respect to the molecular adsorption state follows. Note also the somewhat greater saturation coverage of ethylene obtained on the oxide surface, as judged by the larger area of the adsorbate induced levels.

3. Hydrogen on Carbonated Fe(100)

Figure 4 compares the essential spectral features for acetylene and ethylene chemisorption on the clean surface at 123 K with those obtained by chemisorption of hydrogen onto a carbonated Fe(100) surface at 98 K. The carbonated surface may be prepared either by high temperature hydrocarbon adsorption or by sputter-annealing. The carbon ($2p$) resonance level at ~3 eV is clearly visible in curve 1a, Fig. 4, for which the estimated carbon coverage using Auger electron spectroscopy is approximately one monolayer equivalent (see previous discussion). Adsorption of hydrogen onto this surface gives rise to two new levels at about 7.5 and 11.0 eV (peaks A and B, respectively). For exposures between 50 and 100 L H_2 (curves 1b and 1c, respectively), these levels closely reproduce both the peak shapes and positions of the corresponding levels in the ethylene spectrum (curve 2), if small differences in background intensity are accounted for. The only correlation that can be made with the acetylene spectrum (curve 3) is with peak A, but in this case the peak width and shape are not accurately reproduced. Peak B is absent in the acetylene spectrum; on the other hand, there is a weak level at ~9.3 eV and a broad shoulder-like structure around 4.9 eV. These features are also present in the ethylene spectrum.

4. Adsorption of Acetylene and Ethylene on Partially Deactivated Iron Surfaces

In addition to adsorption on clean Fe(100), acetylene and ethylene were also adsorbed onto partially deactivated Fe(100) surfaces, i.e., carbonated or oxidized surfaces, whose preparation has already been discussed. Figure 5 includes difference spectra for (1) acetylene and (2)

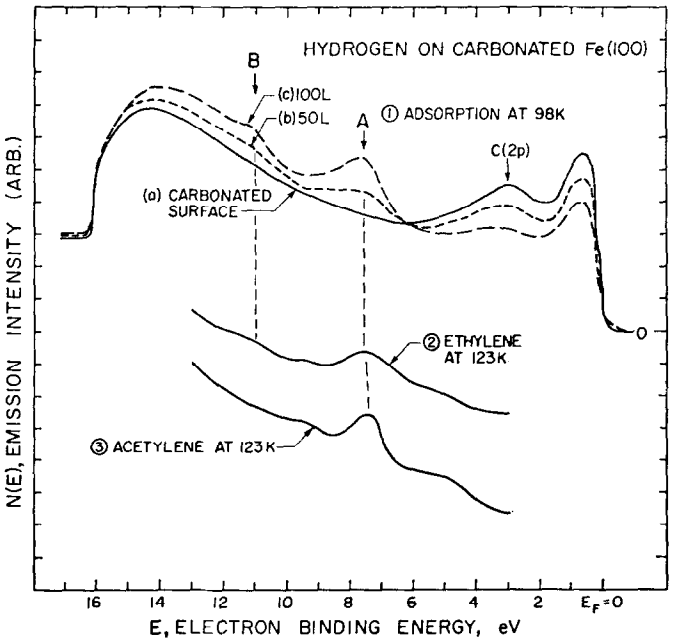

FIG. 4. Comparison of UPS spectral features ($\hbar\omega$ = 21.2 eV) for (1) sequential exposure of a carbonated Fe(100) surface to hydrogen at 98 K, (2) ethylene adsorption on clean Fe(100) at 123 K, and (3) acetylene adsorption on clean Fe(100) at 123 K. Curves (2) and (3) are reproduced segments of curves 2 (Fig. 3) and 3b (Fig. 2), respectively. The preparation and characterization of the carbonated surface is described in the text.

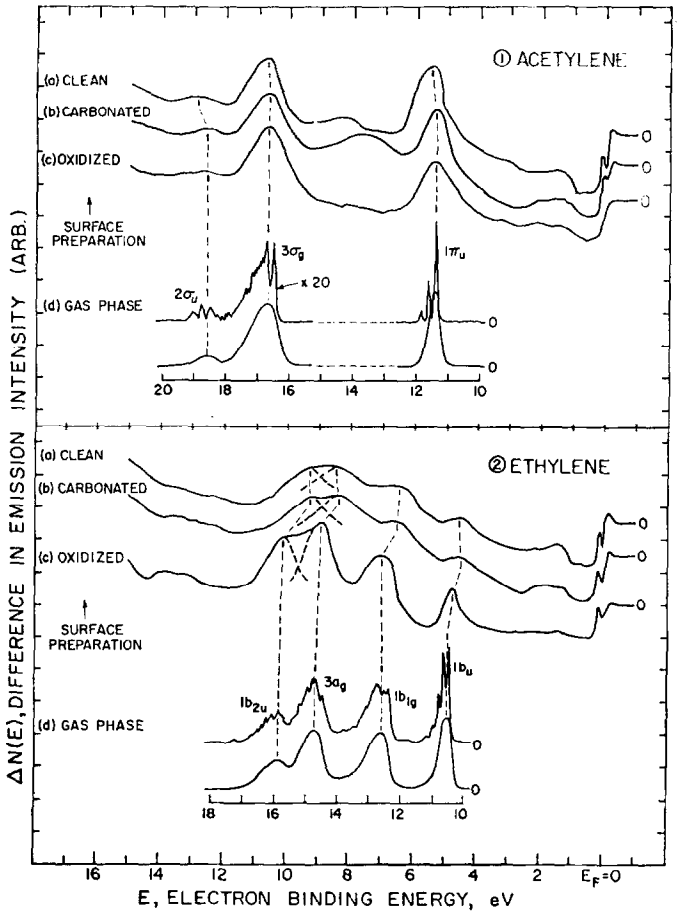

FIG. 5. Difference spectra for (1) acetylene and (2) ethylene adsorbed on the (a) clean, (b) carbonated, and (c) oxidized Fe(100) surfaces at 98 K. Gas phase spectra and molecular orbital designations [from Turner *et al.* (*6*)] included for comparison. Proposed deconvolutions indicated for $3a_g$ and $1b_{2u}$ ethylene levels.

ethylene adsorbed onto the (a) clean, (b) carbonated, and (c) oxidized surfaces. The corresponding unsubstracted spectra can be obtained by addition of each difference curve in Fig. 5 to the appropriate spectrum for the clean (curve 1a, Fig. 2), carbonated (curve 1a, Fig. 4), or oxidized (curve 3a, Fig. 3) surface. The use of difference curves is desirable in the analysis of adsorbate-induced levels especially when locating positions of peaks situated on a steep background. It is significant that precise difference curves obtained digitally using the computer made possible the rendering of subtle features due to adsorption without additional manipulation of the data associated with averaging or interpolation. Also note that all of the adsorbed species in Fig. 5 represent stable phases at 98 K except for acetylene on the clean surface, in which case a gradual conversion process occurs, as previously discussed. In this instance the spectrum was thus recorded as soon as possible after exposure. Lastly, all difference curves are for a single saturation exposure.

For comparison, photoemission spectra at $\hbar\omega = 21.2$ eV for gaseous acetylene and ethylene (*6*) have also been included in Fig. 5. Peak positions for the gas phase

spectra were determined by taking the points of maximum intensity in the hand-smoothed curves shown underneath each spectrum. Each gas phase spectrum was then arbitrarily positioned so as to provide best registry with the appropriate difference curves for adsorption onto the oxide surface. The three occupied valence electronic levels in the acetylene spectrum have assigned the $1\pi_u$, $3\sigma_g$, and $2\sigma_u$ molecular orbital designations after Turner *et al.* (*6*). In the case of ethylene, there is some uncertainty associated with the energetic ordering of the valence orbitals, but recent calculations of excitation probabilities and comparison to XPS results for gaseous ethylene (*6*, *7*) indicate the ordering as shown in Fig. 5. Some confusion also exists over the molecular orbital theoretical labels for the ethylene valence levels, i.e., depending on how the molecular symmetry planes are oriented relative to the *xyz* coordinate system, the same ethylene orbital can assume different labels (*6–9*). For consistency, we follow the notation of Turner *et al.* (*6*), i.e., $1b_u$, $1b_{1g}$, $3a_g$, and $1b_{2u}$.

V. DISCUSSION

An understanding of the modifications in the valence molecular orbital structure which can occur during chemisoption of a gas molecule on a surface is most important. Identification of the adsorbate induced levels is achieved by comparison of the photoemission spectrum of the chemisorbed species to its gaseous or condensed phase counterpart to properly identify the spectral peaks (*10*). In the simplest case, relatively little change in orbital ionization energies can be expected as the gas molecule is brought down to the surface, except for a uniform shift to lower binding energies. This is generally attributed in large part to "relaxation" effects (*11*, *12*).

In contrast to weakly interacting physisorbed or condensed systems, chemisorption usually involves the formation of strong chemical bonds at the surface. Participation of substrate and adsorbate electrons in bonding interactions is reflected by chemical bonding shifts and level broadenings in the chemical fingerprint spectrum. In addition, so-called non-surface bonding adsorbate orbitals may be significantly perturbed in a complicated fashion if the bonding and back-bonding results in a geometrical distortion of the molecule. It is a general objective of this study to achieve insight into this complex problem by systematic investigation of the chemisorptive behavior starting at low temperatures of simple molecules on well-characterized transition metal surfaces.

The chemisorptive behavior of the unsaturated hydrocarbons, acetylene and ethylene, on clean and partially deactivated iron surfaces provides an appropriate test to infer the detailed physical and chemical state of the surface–adsorbate system. Comparisons are also made to the much broader implications of organometallic chemistry, to recent results of cluster chemistry, and to other photoemission studies on transition metal surfaces.

1. Fragmentation on the Clean Fe(100) Surface

The difference spectra of Fig. 5 show a good correspondence with the appropriate gas phase spectra in terms of the relative spacings and amplitudes of the adsorbate-induced levels for both acetylene and ethylene. Thus, for saturated coverages typical of the low temperature regime (Fig. 5), it appears that acetylene and ethylene retain their essential free molecular orbital structure on the surface. There are, however, small but significant perturbations of certain orbitals evident in Fig. 5 related to the geometric distortion (stretching and bending) of the adsorbed molecules. Chemisorptive behavior during the more initial stages of ex-

posure and at higher temperatures gives evidence for much stronger reactive properties.

a. Adsorption of acetylene at low temperature. We consider first the nature of adsorbed acetylene on clean Fe(100) at 123 K (curve 3b, Fig. 2). Previous photoemission measurements for acetylene chemisorbed on Ni(111) (*11*), W(110) (*13*) and on polycrystalline Fe (*14*) and Cu (*14*) films have indicated strong but molecular chemisorptive bonding via the acetylene π-orbitals, the nonbonding $3\sigma_g$ and $2\sigma_u$ orbitals remaining essentially unperturbed by the surface interaction. More recent results for chemisorption on Ir(100) (*15*, *16*) suggest that the π-bonding also involves distortion (stretching and bending) of the chemisorbed molecule under certain conditions, as evidenced by an increased energy separation of the $3\sigma_g$ and $2\sigma_u$ orbitals. The "relaxation" shifts for the $3\sigma_g$ orbital range from 3.0 eV for iridium to 3.5 eV for copper (see Fig. 6). Chemical bonding shifts for the $1\pi_u$ orbital range from 1.2 eV for iridium to 1.9 eV for iron and copper. We might associate the features of curve 3b, Fig. 2, with chemisorbed acetylene by identifying peak B as the $3\sigma_g$ chemisorbed orbital. The weak level at 9.3 eV would then be assigned to the $2\sigma_u$ orbital and the shoulder around 4.9 eV to the $1\pi_u$ orbital, broadened and shifted towards the $3\sigma_g$ orbital by surface bonding interactions.

Such an interpretation is associated, however, with an inordinately large implied "relaxation" shift of 4.8 eV (Fig. 6),

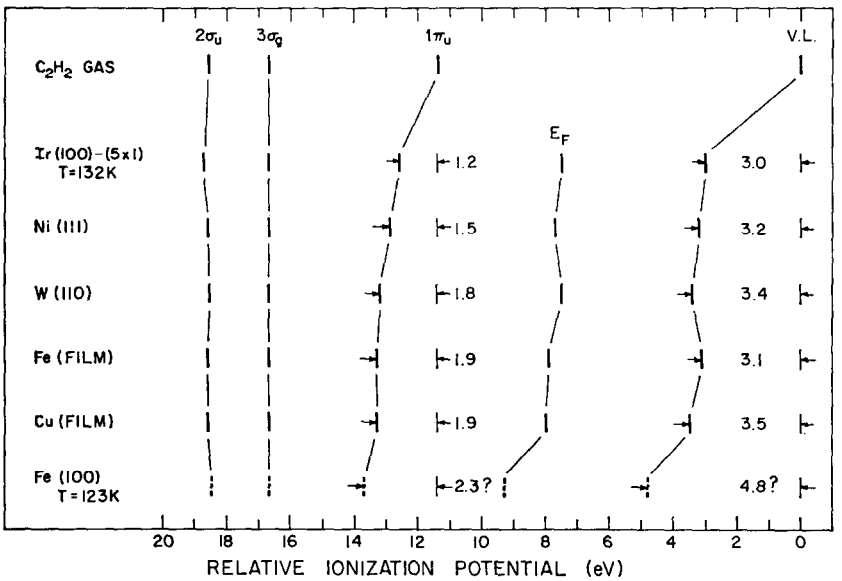

FIG. 6. Comparison of experimentally determined energy levels of gaseous acetylene (*6*) and chemisorbed acetylene on Ir(100) (*15*), Ni(111) (*11*), W(110) (*13*), Fe(Film) (*14*), and Cu(Film) (*14*) to be observed energy levels for acetylene chemisorbed on clean Fe(100) at 123 K (see text). The chemisorbed $3\sigma_g$ levels have been arbitrarily aligned with that of the gas phase. E_F is the Fermi level and V.L. is the vacuum level, the energy difference between them being the measured work function for the saturated surface. "Relaxation" shifts are given by the vacuum level shifts while bonding shifts are given by the shifts of the chemisorbed $1\pi_u$ levels. [Note: We have plotted the vertical ionization potential of each gas phase orbital, which for the $3\sigma_g$ orbital is 16.7 eV (*6*). In Ref. (*13*) comparison was probably made using the adiabatic ionization potential of 16.4 eV for the $3\sigma_g$ orbital. This accounts for some of the differences in the bonding and "relaxation" shifts between this figure and those in Ref. (*13*).]

as well as an unusually large π-bonding shift of 2.7 eV and a compression of the σ levels (*15, 16*). It thus appears unlikely that the photoemission features represent molecular chemisorbed acetylene.

A more likely interpretation attributes peak B in curve 3b, Fig. 2, to chemisorbed CH fragments. It is postulated that this results from π-*d* bonding interactions and stretching of the molecule to such an extent that carbon–carbon scission occurs during chemisorption of acetylene on the clean Fe(100) surface. This behavior is in agreement with calculations by Rhodin *et al.* (*2*). The gradual conversion process (see Fig. 2) appears to be a transformation from the molecular to the fragmented state on the surface. Building up of the peak at 7.5 eV is consistent with the suggestion (*2*) that the CH peak lies approximately midway in energy between the $1\pi_u$ and $3\sigma_g$ peaks (curve 2, Fig. 2). A possible explanation for the 4.9 eV shoulder (curve 3b, Fig. 2) can also be based on the Fe–CH π-bonding interactions (*2*). The origin of the weak level at 9.3 eV remains uncertain.

The presence of apparently weakly bonded acetylene molecules on the clean Fe(100) surface can also be understood as forming above the layer of dissociated acetylene fragments. The residue of peak B (attributed to the chemisorbed CH groups) is consistent with this conclusion (curve 1c, Fig. 2). The iron surface is considered to promote carbon–carbon scission of the adsorbate during initial stages of adsorption. The complex layer of CH fragments and possibly carbon and hydrogen atoms as well (*2*) sufficiently deactivates the iron surface to permit subsequent formation of a more weakly bound molecular layer.

The hypothesis that molecules in close proximity to the clean surface tend to stretch and dissociate provides insight into the possible kinetic mechanisms responsible for the gradual conversion process. Formation of multilayer islands, which grow laterally from perimeter-localized dissociation of acetylene molecules, appears to occur on the clean iron surface. Island formation has been proposed for a wide variety of condensed gases (*12*). The observed constant "relaxation" energy shift of the adsorbate induced peaks is consistent with the fact that the molecules initially condense by an island rather than by a uniform monolayer mechanism (*12*). The coverage dependence of the relaxation shift for acetylene on iron cannot easily be determined but the ethylene on iron system is sufficiently stable to allow sequential exposure measurements to test this hypothesis. Unfortunately for ethylene, the adsorbate-induced levels are not sufficiently sharp to apply the relaxation shift test with certainty. Finally, the possibility of photodissociation of adsorbed molecules by incident uv photons appears unlikely, as tests indicate a negligible cross section for this process.

b. Adsorption of ethylene at low temperature. The adsorptive behavior of ethylene on clean Fe(100) differs from that of acetylene, mainly in the temperature of activation and in the nature of the fragmented species. The UPS spectrum (curve 2, Fig. 3) bears no resemblance to previously reported spectra for chemisorbed ethylene (*11, 13–15*). The possibility of a chemisorbed acetylene species, which might be formed as a result of ethylene dehydrogenation (*11, 13–15*), is also considered to be unlikely.

The spectral features of curve 2, Fig. 3 appear to be characteristic primarily of CH_2 fragments, i.e., methylene radicals. Note that the π_{CH_2} orbital of the chemisorbed methylene radical would be expected to lie approximately half-way in energy between the $1b_{2u}$ and $1b_{1u}$ orbitals of molecularly chemisorbed ethylene (*16*) (composed of bonding and antibonding combinations of π'_{CH_2} components, respectively). From curve 2a, Fig. 5, we locate the midway point between the $1b_{2u}$ and

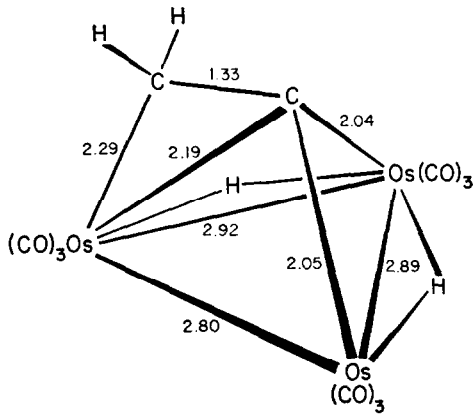

FIG. 7. Illustration of the (CCH_2) mode of interaction for dissociative vinylidene "chemisorption" of ethylene on an osmium cluster. Preliminary crystallographic data from Ref. (*20*).

$1b_{1g}$ peaks at about 7.9 eV, not far from the position of peak E at 7.6 eV in curve 2, Fig. 3. Differences in relaxation shifts can easily account for part of the observed 0.3 eV difference. It is proposed that ethylene molecules absorb on top of the fragmented species, similar to the case of acetylene. Thus, due to the geometric dependence of image charge screening (*18*), a slightly greater relaxation shift might be expected for the specie "closest" to the surface, which we infer to be a "methylene-like" radical. This would shift the π_{CH_2} peak for the methylene-like radical to slightly lower binding energy, as observed.

Convincing evidence for the presence of CH_2 fragments is provided by the essential features of the ethylene spectrum produced during the adsorption of hydrogen onto the carbonated Fe(100) surface (Fig. 4). This result indicates that the combination of H_2 with chemisorbed C atoms forms chemisorbed CH_2 methylene radicals and accounts for the main 7.6 eV level. The presence of the second adsorbate-induced level at 11 eV and recent results of cluster chemistry (*19*) suggest, however, the possibility of other dissociative fragments as well.

Systematic evaluation of cluster chemistry is essential to further development of the cluster–metal surface analogy (*19*). One interesting result of cluster chemistry is the interaction of $Ru_3(CO)_{12}$ and $Os_3(CO)_{12}$ with various types of hydrocarbons (*19, 20*). (Note that ruthenium and osmium lie directly beneath iron in the Periodic Table.) The propensity of the osmium cluster to break C–H and C–C bonds is well known. A formal analogy with the chemisorptive reaction on metal surfaces is proposed. For its hydrocarbon reactions with ethylene, the product has the stoichiometric composition $Os_3(CO)_9$-C_2H_4, but there are structural isomers. In one isomer, $H_2Os_3(CO)_9CCH_2$, there are two hydrogen atoms bonded to osmium and only one carbon atom bears hydrogen atoms, as illustrated in Fig. 7. A second structural isomer, $H_2Os_3(CO)_9HCCH$, has one hydrogen atom bonded to each carbon atom in the usual sense, i.e., coordinated acetylene. These results illustrate the important question [previously indicated in Refs. (*19, 20*)] as to whether dissociative adsorption of ethylene on metal surfaces involves a two-hydrogen atom loss from a single carbon atom, as in this cluster isomer case, or a one-hydrogen atom loss from both carbon atoms. We cannot rule out the possibility that both modes of interaction may occur on metal surfaces. It has been concluded that the main spectral features of curve 2, Fig. 4, are not typical of chemisorbed acetylene. The presence of a chemical phase possibly unique to surface complexes, such as vinylidene (CCH_2), is suggested. The broad level at ~11 eV would then be associated with delocalized residual carbon–carbon σ-bonding in the vinylidene fragment. This leads to the interesting consequence that chemisorbed hydrogen molecules on the carbonated surface induce bonding interactions between the carbon atoms.

The reactivity of iron, ruthenium and other transition metal surfaces towards chemisorbed CO has been interpreted in terms of photoemission spectra [see Ref.

(*21*) and references cited therein] involving the concept that transition metal surfaces stretch and dissociate the chemisorbed CO molecule. This tendency is observed to increase as one moves upwards (and leftwards) from platinum in the Periodic Table. Thus, Fe(100) dissociates chemisorbed CO at room temperature (*21*, *22*), whereas Ru(1010) does not (*21*, *23*). This serves to emphasize the significance of ruthenium and osmium surface chemistry to that of iron, since the stretching phenomenon in coordinated CO and unsaturated hydrocarbons is due to analogous π-back-bonding mechanisms (see discussion on stretching below). The same enhanced chemical reactivity of iron towards hydrocarbons, relative to ruthenium and osmium, would be expected as was found for CO. It should be noted however, the greater importance of the surface geometric factor on the chemisorptive behavior of hydrocarbons (*15*, *16*).

The mechanism of conversion from the molecular to the fragmented state of adsorbed ethylene is analogous to that proposed for acetylene, but with a somewhat higher activation energy. The peak E (curve 1b, Fig. 3), characteristic of the fragmented molecule, is again observed during initial exposure. It is considered that valence orbitals of the various fragmented species interact with metallic *d*-orbitals, forming an intimately complexed partially deactivated surface layer. Ethylene molecules are subsequently weakly held on top. It appears that at 98 K the multilayer structure is "frozen" in. Upon warming to 108 K, activated migration and dissociative interaction of loosely bound ethylene molecules to uncomplexed surface sites occurs.

2. *Molecular Adsorption on Partially Deactivated Fe(100) Surfaces*

a. Patterns of bonding in metal–olefin complexes. The most widely accepted model

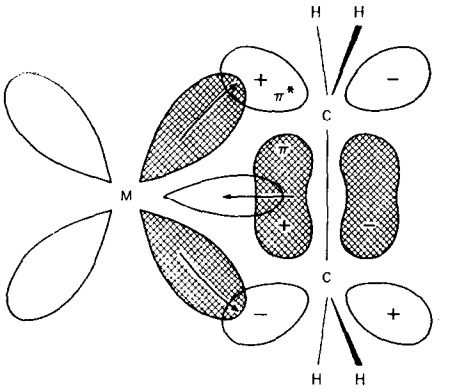

FIG. 8. The Dewar–Chatt–Duncanson molecular orbital picture of bonding between ethylene and a metal ion. Shaded orbitals are fully occupied, unshaded orbitals unoccupied. Arrows indicate forward (←) and back (→) bonding donations.

for the patterns of bonding in metal–olefin complexes is that proposed by Dewar (*24*) and by Chatt and Duncanson (*25*). This model (Fig. 8), involving formation of a σ-bond by donation of π-electrons to the metal atom and formation of a π-bond by back donation from the *d*-orbitals of the metal to the olefin π^* orbital, is useful in discussing the reactivity of iron surfaces towards acetylene and ethylene. Especially relevant to our discussion is the lengthening of the carbon–carbon bond (*26*, *27*, *34*, *35–37*) in the coordinated molecule, a consequence of the forward and back donation processes which tend to weaken the carbon–carbon bond. Another important aspect of coordination geometry is the bending of the substituent groups away from the metal atom as the π^* orbital becomes appreciably populated (*26–29*, *36*, *37*). The relative significance of σ vs π contributions to the overall bonding has been investigated in several recent detailed calculations on the bonding of unsaturated molecules to transition metals (*30–32*). For a thorough discussion of these and other aspects of organometallic bonding interactions, the reader is referred to the review by Ittel and Ibers (*33*).

For the detection of subtle differences within a given series of compounds, spec-

troscopic techniques such as X-ray photoemission spectroscopy (*38, 39*) and infrared spectroscopy (*40–42*) have generally been more useful than diffraction studies. Unequivocal information on the nature of the all-important bonding interactions of the unsaturated molecule with the transition metal still remains limited. However, with the advent of uv-photoemission spectroscopy, the interactions of valence electrons involved in chemical bonding can now be probed directly. Significant details of molecular orbital involvement in bonding interactions of acetylene and ethylene on iron surfaces are readily ascertained from the photoemission spectra.

b. π-d Bonding interactions and molecular distortion. Evidence for stretching effects during the chemisorption of acetylene and ethylene on deactivated Fe(100) surfaces is found in perturbations of the lower lying valence σ-orbitals not directly involved in bonding interactions with the substrate. It has been demonstrated in chemisorption studies on Ir(100) surfaces (*15, 16, 21*) that adsorbate valence orbitals, accessible in a photoemission experiment and not directly involved in surface bonding interactions, can provide information on changes in the geometrical nature of the adsorbed vs the free molecule. The method, which represents a significant extension of the "fingerprint" technique (*10*), has general applicability provided the essential nature of the bonding interactions are understood, the rough spatial and density distributions of the molecular orbitals have been worked out, and the appropriate gas phase spectrum is available for comparison. Recent results for W(100) (*43*) also show evidence for stretching effects. Based on the results for iridium and tungsten, it is apparent that the stretching tendency of chemisorbed acetylene and ethylene is a sensitive function of both geometric and electronic surface factors, in contrast to the chemisorptive stretching behavior of CO where the electronic surface factor is clearly dominant (*21*).

The valence molecular orbitals for free acetylene and ethylene molecules are schematically indicated in Fig. 9, which also shows the experimentally observed peak positions of Fig. 5 replotted for greater ease of comparison with gas phase ionization potentials. Alignment of the ionization potentials has been done for the $3\sigma_g$ orbital of acetylene, and the $3a_u$ orbital of ethylene. Note that the weak chemisorption bonding shift of the bonding π orbital is only $\lesssim$0.2 eV. This contrasts to bonding shifts of 1.2–1.9 eV for the $1\pi_u$ orbital of chemisorbed acetylene (see Fig. 6) and 0.6–1.0 eV for the $1b_{1u}$ orbital of chemisorbed ethylene (*11, 14, 16*). The bonding shifts corresponding to weak chemisorption are always much smaller than those observed for strong chemisorption on clean transition metal surfaces.

Significant variations in the relative spacings of the non-surface-bonding σ levels are apparent in Fig. 9. An expansion or a compression of the σ-level manifold of acetylene or ethylene, respectively, in comparison to the gas phase spacing, implies a stretching of the molecular carbon–carbon bond, assuming no direct interactions between the σ orbitals and the substrate (*15, 16*). In stretching the carbon–carbon bond, an orbital which is bonding with respect to the two carbon atoms shifts to lower binding energy, while an antibonding orbital moves to greater binding energy. For example, the C–C antibonding $2\sigma_u$ orbital of acetylene "benefits" from the decreased overlap and increases its binding energy, whereas the primarily C–C bonding $3\sigma_g$ orbital loses stability as the overlap is diminished and moves to smaller binding energy (see Fig. 9). The net effect of stretching is thus an increase in energy separation of the two orbitals. In a similar manner it can be shown for ethylene that a decrease in energy separation between the $1b_{2u}$

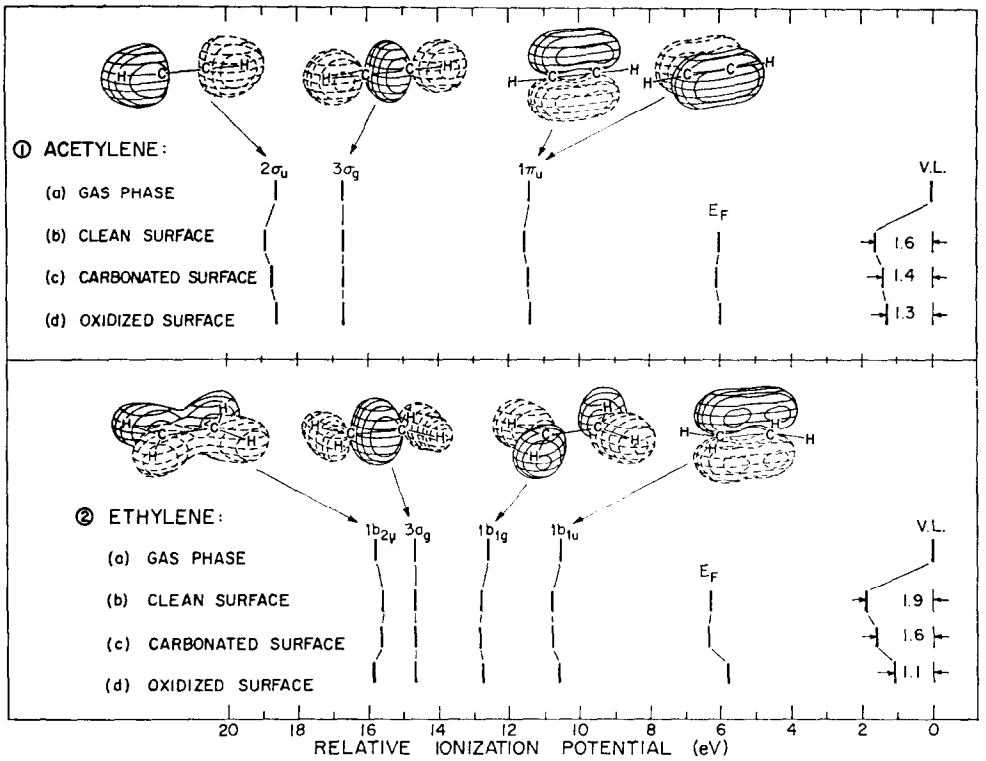

FIG. 9. Comparison of experimentally determined gas phase energy levels of acetylene and ethylene to those observed for acetylene and ethylene weakly chemisorbed on partially deactivated Fe(100) surfaces. Vertical ionization energies are used. The clean surface is self-deactivating due to the fragmentation of initially incident molecules, as explained in the text. Characterization of the carbon- and oxygen-deactivated surfaces is also described in the text. The labeling of the ethylene orbitals is according to Ref. (*6*). The $3\sigma_g$ or $3a_g$ orbitals of weakly chemisorbed acetylene or ethylene, respectively, have all been arbitrarily aligned with that of the gas phase. E_F is the Fermi level and V.L. is the vacuum level, the energy difference between them being the measured work function for the saturated surface. "Relaxation" shifts are given by the vacuum level shifts. The molecular orbital contour plots are redrawn from Ref. (*17*). Solid contours correspond to a positive orbital amplitude, broken contours to a negative orbital amplitude.

(primarily C–C bonding) and $1b_{1g}$ (C–C antibonding) orbitals results upon stretching.

These results are in good agreement with the experimentally observed peak separations for weakly chemisorbed acetylene and ethylene. The relative magnitudes of the observed σ-manifold variation can be used as a gauge of the degree of stretching found on the various surfaces. Thus, the stretching of acetylene is seen to be greatest on the clean surface (which is partially deactivated by the presence of fragments), slightly less on the carbonated surface, and virtually negligible on the oxidized surface (Fig. 9). In the case of ethylene, the stretching is comparable on the clean (but fragment deactivated) and carbonated surfaces, but again, almost negligible on the oxidized surface. We attribute these stretching effects primarily to π^* back-bonding donations into the unfilled antibonding orbitals of the weakly chemisorbed molecules (the π-forward bonding donations may also contribute). It is therefore likely that the stretched molecules are bent as well. Recent model calculations for acetylene and ethylene

show that a σ-manifold expansion and compression, respectively, is consistent with both a stretching and a bending (*44*, *45*).

Trends in the observed "relaxation" shift of the orbital ionization energies (Fig. 9) run parallel to trends in the stretching effect. For acetylene it is thus greatest on the clean surface, slightly less on the carbonated surface, and least on the oxidized surface. It can be understood from the photohole screening effect being divided into two contributions, electronic charge in surrounding molecules, and mobile conduction electrons in the substrate. The first can be assumed to stay constant since the coverage is approximately the same on each surface. The second would be expected to vary with the density and mobility of conduction d-electrons. More electronegative chemisorbed oxygen atoms are more effective than chemisorbed carbon atoms in depleting iron d-band emission near E_F (compare curves 3a, Fig. 3 and 1a, Fig. 4). Correspondingly, the oxidized surface is seen to be less effective in screening the photohole. For the clean and carbonated surfaces it is likely that the coverage of carbon atoms in the intermediate fragmented layer is less than on the carbonated surface. This would explain the relatively greater ability of the clean surface to screen the photohole. Similar parallel trends in stretching and relaxation are observed for weakly chemisorbed ethylene.

In summary, the greatest stretching effects occur on those surfaces showing the largest relaxation shifts. With respect to acetylene and ethylene on iron this implies that the ability of the surface to donate electrons in π^*-back-bonding interactions increases as its ability to screen the photohole. A more detailed interpretation of these results in terms of calculations of the energy levels for various surface–molecule combinations will be discussed in a subsequent paper (*2*).

CONCLUSIONS

π-d forward- and back-bonding interactions for chemisorption on clean iron weaken and stretch the carbon–carbon bond for simple olefins to such an extent that carbon–carbon scission is induced. Chemisorptive fragments appear to be mainly of the CH_n (n = 1, 2) type, with the possibility of CCH_2 and other fragmented species.

Chemisorptive bonding interactions are moderated by controlled partial deactivation of the surface, providing insight into the relationship between the surface electronic structure and the observed reactivity of the surface. It also sheds light on the ubiquitous but poorly understood "relaxation" phenomenon accompanying photoemission from chemisorbed species.

The Fe(100) surface is also found to be more reactive towards carbon monoxide than other metals, either below or to the right of iron in the Periodic Table. Smoothly varying trends in reactivity as a function of position in the Periodic Table are, however, not found for chemisorbed hydrocarbons due to the increased importance of the geometric vs the electronic surface factor.

ACKNOWLEDGMENTS

Research support from the Cornell University Materials Science Center and from the American Iron and Steel Institute is gratefully acknowledged. The authors thank G. Brodén and A. B. Anderson for helpful discussions of this work and of their own prior to publication. One of the authors (C. F. B.) is grateful for partial scholarship support from the American Vacuum Society. We also thank B. F. Addis of the Cornell MSC Crystal Growth Facility for preparing the iron single crystal.

REFERENCES

1. Anderson, A. B., Rhodin, T. N., and Brucker, C. F., *Bull. Am. Phys. Soc.* **21** (7), 940 (1976).
2. Rhodin, T. N., Anderson, A. B., and Brucker, C. F., to be published.
3. Brucker, C. F., and Rhodin, T. N., *Surface Sci.* **57**, 523 (1976).

4. Legg, K. O., Jona, F. P., Jepson, D. W., and Marcus, P. M., *J. Phys. C* **8**, L492 (1975).
5. Hagstrum, H. D., private communication.
6. Turner, D. W., Baker, C., Baker, A. D., and Brundle, C. R., "Molecular Photoelectron Spectroscopy," pp. 167, 179, 190. Wiley (Interscience), London, 1970.
7. Berndtsson, A., Basilier, E., Gelius U., Hedman, J., Klasson, M., Nilsson, R., Mordling, C., and Svensson, S., *Physica Scripta* **12**, 235 (1975).
8. Mulliken, R. S., *J. Chem. Phys.* **23**, 1997 (1955).
9. Palke, W. E., and Kipscomb, W. N., *J. Amer. Chem. Soc.* **88**, 2384 (1966).
10. Rhodin, T. N., and Brucker, C. F., *in* "Proceedings of the Symposium on Advances in Characterization of Metal and Polymer Surfaces" (L. H. Lee, Ed.). Academic Press, New York, 1977.
11. Demuth, J. E., and Eastman, D. E., *Phys. Rev. Lett.* **32**, 1123 (1974).
12. Yu, K. Y., McMenamin, J. C., and Spicer, W. E., *Surface Sci.* **50**, 149 (1975).
13. Plummer, E. W., Waclawski, B. J., and Vorburger, T. V., *Chem. Phys. Lett.* **28**, 510 (1974).
14. Yu, K. Y., Spicer, W. E., Lindau, I., Ianetta, P., and Lin, S. F., *J. Vac. Sci. Technol.* **13**, 277 (1976).
15. Brodén, G., and Rhodin, T. N., *Chem. Phys. Lett.* **40**, 247 (1976).
16. Brodén, G., Rhodin, T., and Capehart, W., *Surface Sci.* **61**, 143 (1976).
17. Jorgensen, W. L., and Salem, L., "The Organic Chemist's Book of Orbitals," pp. 73, 74. Academic Press, New York, 1973.
18. Gadzuk, J. W., *J. Vac. Sci. Technol.* **12**, 289 (1975).
19. See for example, the recent review by Muetterties, E. L., *Bull. Soc. Chim. Belg.* **84**, 959 (1975), and references cited therein.
20. Deeming, A. J., and Underhill, M., *J. Chem. Soc. Chem. Commun.* 277 (1973).
21. Brodén, G., Rhodin, T. N., Brucker, C. F., Benbow, R., and Hurych, Z., *Surface Sci.* **59**, 593 (1976).
22. Rhodin, T. N., and Brucker, C. F., unpublished data.
23. Fuggle, J. C., Madey, T. E., Steinkilberg, M., and Menzel, D., *Surface Sci.* **52**, 521 (1975).
24. Dewar, M. J. S., *Bull. Soc. Chim.* **18**, C71 (1951).
25. Chatt, J., and Duncanson, L. A., *J. Chem. Soc.* 2939 (1953).
26. Blizzard, A. C., and Santry, F. P., *J. Amer. Chem. Soc.* **90**, 5749 (1968).
27. Orgel, L. E., "Introduction to Transition-Metal Chemistry," p. 137. Methuen, London, 1960.
28. Nelson, J. H., and Jonassen, J. B., *Coord. Chem. Rev.* **6**, 27, 40 (1971).
29. Hartley, F. R., *Chem. Rev.* **69**, 799 (1969).
30. Rosch, N., and Rhodin, T. N., *Phys. Rev. Lett.* **32**, 1189 (1974).
31. Rosch, N., Messmer, R. P., and Johnson, K. H., *J. Amer. Chem. Soc.* **96**, 3855 (1974).
32. Norman, J. G., *J. Amer. Chem. Soc.* **96**, 3327 (1974).
33. Ittel, S. D., and Ibers, J. A., *in* "Advances in Organometallic Chemistry" (F. G. A. Stone and R. West, Eds.), Vol. 14, pp. 33–61. Academic Press, New York, 1976.
34. Davis, M. I., and Speed, C. S., *J. Organometal. Chem.* **21**, 401 (1970).
35. "Tables of Interatomic Distances and Configuration in Molecules and Ions," Supplement (L. E. Sutton, Ed.), Special Publication No. 18. Chem. Soc., London, 1965.
36. Stalick, J., and Ibers, J., *J. Amer. Chem. Soc.* **92**, 5333 (1970).
37. Nelson, J. H., Wheelock, K. S., Cusachs, L. C., and Jonassen, H. B., *J. Amer. Chem. Soc.* **91**, 7005 (1969).
38. Cook, C. D., Wan, K. Y., Gelius, U., Hamrin, K., Johansson, G., Olsson, E., Siegbahn, H., Nordling, C., and Siegbhan, K., *J. Amer. Chem. Soc.* **93**, 1904 (1971).
39. Brant, P., Enemark, J. H., and Balch, A. L., *J. Organometal. Chem.* **114**, 99 (1976).
40. Ittel, S. D., and Ibers, J. A., *J. Organometal. Chem.* **57**, 389 (1973).
41. Quinn, H. W., and Tsai, J. H., *Advan. Inorg. Chem. Radiochem.* **12**, 217 (1969).
42. Tolman, C. A., *J. Amer. Chem. Soc.* **96**, 2780 (1974).
43. Waclawski, B. J., and Vorburger, T. V., Prog. 36th. Annu. Conf. Phys. Electronics, p. T2.4, June 7–9 1976.
44. Demuth, J. E., and Eastman, D. E., *Phys. Rev.* B **13**, 1523 (1976).
45. Goddard, W., private communication.